Case Studies in Construction Materials 22 (2025) e04397

Contents lists available at ScienceDirect

Case Studies in Construction Materials

journal homepage: www.elsevier.com/locate/cscm

Experimental study on engineering properties of weathered phyllite filler with different gravel contents

Yanjie Zhang [a,*], Weizhong Lai [a], Xu Wang [a,b], Hanxing Zhu [c], Liang An [d,e]

[a] School of Civil Engineering, Lanzhou Jiaotong University, Lanzhou 730070, China
[b] National and Provincial Joint Engineering Laboratory of Road &Bridge Disaster Prevention and Control, Lanzhou Jiaotong University, Lanzhou 730070, China
[c] School of Engineering, Cardiff University, Cardiff CF24 3AA, UK
[d] Gansu Province Transportation Planning, Survey & Design Institute CO. LTD., Lanzhou 730030, China
[e] College of Earth and Environmental Sciences, Lanzhou University, Lanzhou 730000, China

ARTICLE INFO

Keywords:
Weathered phyllite
Subgrade filler
Gravel content
Compaction
Mechanical properties
Hydraulic characteristics

ABSTRACT

The use of weathered phyllite waste slags generated from the excavation of cuttings and tunnels as roadbed filler material can effectively address issues related to filler scarcity, environmental protection, and cost. This study focused on weathered phyllite obtained from a highway expansion project in the Longnan Area of Gansu Province, China. Various experiments were conducted in a laboratory setting, including compaction, unconfined compressive strength (UCS), California bearing ratio (CBR), permeability, and disintegration tests, to investigate the response of mixtures with different gravel contents (GCs), ranging between 30 %–70 % by weight of weathered phyllite filler (WPF). The test results indicate the presence of a critical GC threshold. At 55 % GC, the WPF exhibits optimal compaction, the highest UCS and CBR values, and the lowest permeability and disintegration rates. Upon reaching this critical GC threshold, the phyllite gravels contact each other to form a skeletal structure, while fine grains fill the gaps within this structure to create a denser skeleton configuration. Coarse phyllite gravels are more prone to fragmentation into finer grains, which can effectively occupy large, medium, and small voids between particles. Consequently, the WPF exhibits enhanced structural density and improved mechanical and hydraulic properties. These findings provide a theoretical reference for the engineering application of phyllite in mountainous projects.

1. Introduction

The reuse of waste rock blocks (WRB) is a matter of global concern and significant international interest. The urgent need to repurpose WRB is primarily driven by environmental considerations stemming from the increasing scarcity of natural resources and the rising costs of landfill in many countries[1–4]. The sustainable application of traditionally discarded WRB in civil engineering has generated considerable interest in recent years. Research by various authors has explored the use of recycled WRB in road and pavement applications. The existing literature on employing WRB as a road construction material can be categorized into four groups [5]: (i) WRB used directly without treatment; (ii) WRB stabilized with hydraulic binders (cement/lime) with or without the presence of soil/clay; (iii) WRB stabilized through the geopolymerization process; and (iv) WRB combined with asphalt. Table 1 summarizes the

* Corresponding author.
E-mail address: zhangyanjie@lzjtu.edu.cn (Y. Zhang).

https://doi.org/10.1016/j.cscm.2025.e04397
Received 1 May 2024; Received in revised form 19 January 2025; Accepted 10 February 2025
Available online 11 February 2025

use of WRB as road construction materials. Key design criteria for WRB structures include mechanical strength, workability, environmental performance, hydraulic conductivity, and durability. Various geotechnical property tests (GPTs), including proctor compaction test (PCT), unconfined compressive strength (UCS), California bearing ratio (CBR), X-ray diffraction (XRD), mercury intrusion porosimetry (MIP), scanning electron microscopy (SEM), and assessments of durability and leaching characteristics were conducted.

In the central and western regions of China, substantial quantities of phyllite, a regional metamorphic soft rock, have been revealed [20–22]. With the continuous highway construction in mountainous areas, geological disparities have increased the number of tunnels and road cutting. Consequently, the abundant waste slags from phyllite not only incur in transportation costs during construction but also contribute to environmental pollution and ecological damage. To control project costs while adhering to environmentally friendly principles in highway designs that utilize locally sourced materials, extensive waste slags from soft rocks have been utilized as roadbed filler material, resulting in significant economic and environmental benefits [23–27].

Phyllite is a low-grade metamorphic rock exhibiting a degree of metamorphism between slate and schist and is characterized by its phyllitic structure [28]. Owing to prolonged weathering and seismic activity, phyllite possesses attributes such as diminished strength, weak cementation, and disaggregation upon contact with water. Consequently, soft rocks such as phyllite are considered unsuitable for use as roadbed filler in the current specifications pertaining to road engineering construction [29,30]. The engineering properties of weathered phyllite can be enhanced by applying cement or lime, and some studies have reported successful outcomes [20,29–32]. However, these improvements are associated with significant environmental pollution [33]. It is widely acknowledged that lime and cement production results in substantial greenhouse gas emissions [34]. According to previous studies, the production of each ton of lime releases 1.2 tons of carbon dioxide, while for every ton of cement produced 0.8 tons of carbon dioxide are emitted [35]. Currently, sustainable development and the conservation of natural resources are globally prioritized concerns, necessitating the exploration of alternative approaches [36,37].

Soil and gravel mixtures (SGMs) are comprised of gravels of varying sizes and fine-grained soil [38,39]. In this context, "gravel" is

Table 1
WRB used as road construction materials.

References	Site	Type of WRB	Treated methods	Conducted tests	Properties use
[6]	Melbourne, Australia	Electric arc furnace slag, ladle furnace slag	Without treatment	GPTs, organic content, pH, , CBR, total and leachable heavy metal tests.	Ladle furnace slag is ideal for usage as a construction material in roadwork applications and engineering fills. Electric arc furnace slag is suitable to use as a construction material for pavement subbases and engineering fills.
[7]	Morocco	Phosphate mine waste rocks		In situ tests, double oedometer tests, triaxial tests, MIP, XRD.	Phosphate mine waste rocks can be used for the construction of dry compacted embankments. The embankment exhibited significant bearing capacity and showed satisfactory dry density.
[8,9]	Turkey	Waste limestone powder		UCS,CBR,1-D consolidation	Possible use of limestone powder for different geotechnical applications including road pavement design is considered.
[10]	Bechar, Algeria	Coal mine tailings		GPTs, PCT, leaching tests, CBR, in situ tests	Coal mine tailings can be used as road base material with a percentage of 25 % completed by local tuff.
[11]	Turkey	Rounded narli gravel, angular crushed rock gravel		CBR, UCS, PCT, 1-D consolidation	Behavior of clay with gravel size aggregate mixtures depends on the grain shape and content of the gravels with same mineralogy and size.
[12]	India	Overburden waste rock		GPTs,consolidation tests, direct shear tests,triaxial shear tests.	Overburden waste rock material in base and subbase layer is significantly more sustainable than the use of natural aggregates.
[13]	Warsaw, Poland	Washed mineral waste		GPTs, permeability tests, direct shear tests.	Washed mineral waste as soil for the backfill of installation trenches, abutments and retaining structures.
[14]	Nigeria	Blackcotton soil	Hydraulic treatment	PCT, UCS, CBR, SEM	Treatment of blackcotton soil for use as sub base material in the construction of low volume roads.
[15]	Brazil	Gold tailings		UCS, pulse velocity tests, durability tests.	UCS of 1.8 MPa was achieved for the mix.
[16]	Morocco	Phosphogypsum		pH, PCT, SEM, CBR, UCS, direct shear test, oedometer tests.	Large quantities of phosphogypsum material can be valorized in various layers of the road construction obviously inside the profitability perimeter.
[17]	Salem, India	Magnesite mine tailings		UCS, CBR, XRD, SEM.	8 % ordinary Portland cement and magnesite mine tailings mix can be used as a subgrade.
[18]	Tucson, Arizona	Copper mine tailings	Geopolymerization treatment	UCS, SEM, XRD.	By selecting appropriate moisture content and NaOH concentration, the geopolymerized copper mine tailings can meet the strength requirements for road base.
[19]	Morocco	Phosphate waste	Bituminous treatment	XRD, viscous flow tests, frequency and temperature sweep tests.	By using 5 % of waste fillers can enhance the rutting resistance performance of the original asphalt binder.

defined solely based on particle size, referring to gravels that are coarser than the soil matrix [40]. The gravel content (GC) is a crucial parameter that influences the physical and mechanical behavior of an SGM [41–45]. In recent years, numerous tests have been conducted to characterize the influence of GC on strength and deformation. Vallejo [46] indicated that when the GC ranged between 40 % and 70 %, both coarse gravels and fine grains collectively contributed to supporting the mixture structure. Gao et al. [47] revealed significant effects on the internal friction angle and cohesion before reaching a critical GC threshold of 70 %. Wang et al. [48] suggested that geomaterials with GC of 50 % exhibited considerably higher strength those with other contents. Cen et al. [38] observed an increase in the peak shear stress and internal friction angle of the interphase, while a decrease in cohesion was noted with an increase in GC. Wang et al. [45] concluded that a higher GC consistently led to a more significant enhancement in the strength and deformation parameters. Zhang et al. [43] investigated the nonlinear relationship between the SGM shear strength and GC, and proposed an empirical formula for predicting the SGM shear strength. Zhang et al. [49] determined that SGM exhibits the highest degree of block contact and interlocks with 60 % GC. According to the particle density theory, an ideal GC can effectively occupy the void spaces within waste rocks, resulting in a mixture with maximum density and strength [50]. The influence of increasing GC on strength varies at different stages, with distinct thresholds observed for variations in strength. Gravels contribute to the friction and overall material strength. However, an increase in GC leads to a greater number of soil-gravel contact faces [43].

Despite recent advancements, previous studies have primarily focused on natural SGM, such as colluvium, eluvium, and diluvium [44,51–54]. However, limited research has been conducted on SGM formed via artificial excavation or blasting [30,40,55]. Liu et al. [40] proposed the use of relative fractal dimensions to evaluate the impact of initial GC on particle breakage in weathered phyllite. Xu et al. [55] found that improved red bed subgrade fillers with 50 % GC exhibited superior mechanical performance and deformation characteristics; this finding was supported by Zhao et al. [30]. Phyllite waste is classified as a type of SGM. Moreover, the filling process of weathered phyllite is accompanied by a series of processes such as particle sliding, crushing, filling and rearrangement. Particle fragments significantly change particle strength, deformation and particle size distribution (PSD) [56]. Therefore, it is imperative to investigate the impact of GC on the physical and mechanical properties to ascertain the suitability of weathered phyllite as a potential filler material for roadbed applications.

In summary, weathered phyllite with unfavorable engineering properties can be utilized as a roadbed filler material after appropriate treatment. Conventional hydraulic treatment techniques may have detrimental effects on the environment. However,

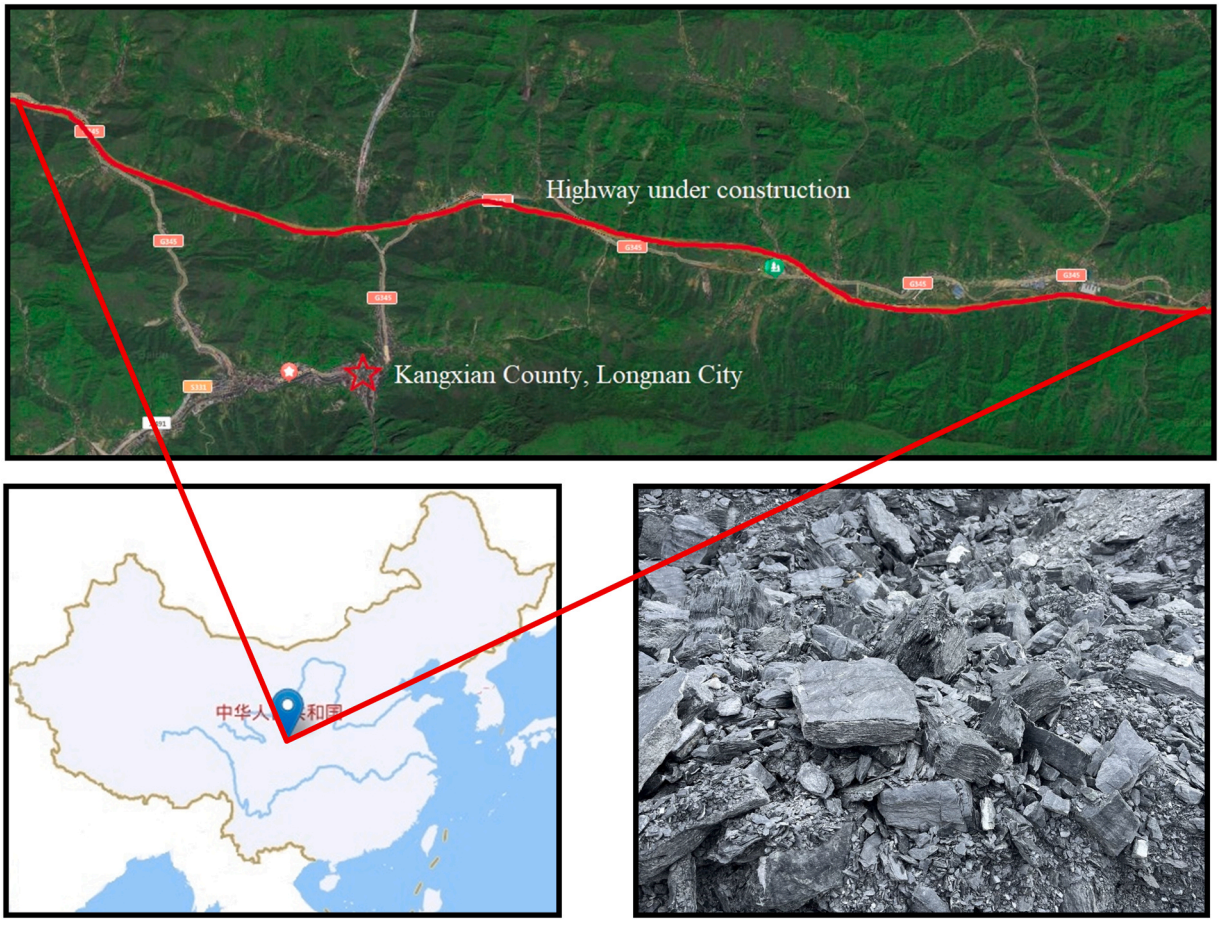

Fig. 1. Location of weathered phyllite filler being studied.

compaction treatment can effectively address both environmental protection and engineering requirements. Previous studies have conducted limited investigations into the engineering properties of phyllite with varying GC, while the hydraulic characteristics of weathered phyllite filler (WPF) remain uncertain. As discussed above, this paper initially examines the basic properties of weathered phyllite materials, including mineral and chemical compositions, microstructure, and physical properties. Subsequently, WPF specimens were prepared by incorporating varying ratios of GC (30 %, 40 %, 50 %, 55 %, 60 %, and 70 % by dry weight). A comprehensive series of laboratory experiments, encompassing standard test for laboratory compaction, UCS, CBR, permeability, and disintegration tests, were conducted to evaluate the performance of the WPF samples. Based on this research, a critical GC threshold was determined, indicating that WPF exhibits enhanced structural density and improved mechanical and hydraulic properties. These findings are expected to increase the suitability of phyllite waste slags as roadbed filler materials in mountainous areas and provide valuable insights for engineering applications.

2. Materials and methods

2.1. Basic properties of weathered phyllite filler

The WPF samples were collected from a highway construction project in the Longnan Area of Gansu Province, China (Fig. 1). The raw gravel was crushed and sieved through a 75-μm mesh (No. 200). In this study, following previous similar investigations [51,57,58], a particle size threshold of 5 mm was selected to distinguish between coarse gravels and fine grains; specifically, particles larger than 5 mm were defined as gravels (or coarse grains), while particles smaller than 5 mm were classified as fine grains.

XRD was performed to determine the mineralogy of the weathered phyllite. Following the methodology described by Garzón et al. [59], a representative sample was crushed and sieved through a 75-μm mesh. Subsequently, the powdered sample underwent drying at 110 °C for 24 h. The results are shown in Fig. 2. The WPF mineral composition was characterized by significant proportions of muscovite (38.0 %), orthoclase (27.1 %), kaolinite (22.5 %), and quartz (12.4 %). Notably, unlike phyllites found in other regions, weathered phyllite exhibits elevated concentrations of muscovite and orthoclase and relatively lower levels of quartz [20,21,30,40,59].

The chemical composition of the sample, as determined via X-ray fluorescence (XRF) analysis (Table 2), was in excellent agreement with the mineralogical composition observed via XRD analysis. The results, expressed in terms of oxide percentages, validate the presence of silica (59.0 %) and alumina (24.1 %) originating from silicate and quartz content, alongside alkaline elements primarily associated with kaolinite and orthoclase content, notably potassium oxide. Noteworthy constituents include iron oxide at approximately 4.8 % as well as magnesium and sodium oxides at similar levels (both approximately 5.61 %), constituting the remaining components at a proportion of 1.77 %. Fig. 3 shows a scanning electron micrograph (SEM) capturing the layered morphologies within weathered phyllite due to the presence of muscovite.

The moisture content and bulk density of the phyllite slag excavated from the tunnel was directly tested. The Atterberg limits of fine particles less than 0.075 mm was measured indoors. The physical properties of weathered phyllite were determined following the guidelines provided by ASTM D2216 [60], ASTM D7263 [61], and ASTM D4318 [62] respectively. The obtained results are presented in Table 3.

Typical gravels were selected, and data regarding the long axis (L), intermediate axis (I), and short axis (S) of the particles were obtained using a 3D laser scanning system. According to the classification of particle shape by Lanaro and Tolppanen [63], as illustrated in Fig. 4, the shapes of the gravels are classified and counted, as shown in Fig. 5. Most phyllite gravels exhibit a flat shape ($S/I < 0.67$, $I/L > 0.67$), some are classified as spherical, while a small proportion may exhibit flake and cubic shape.

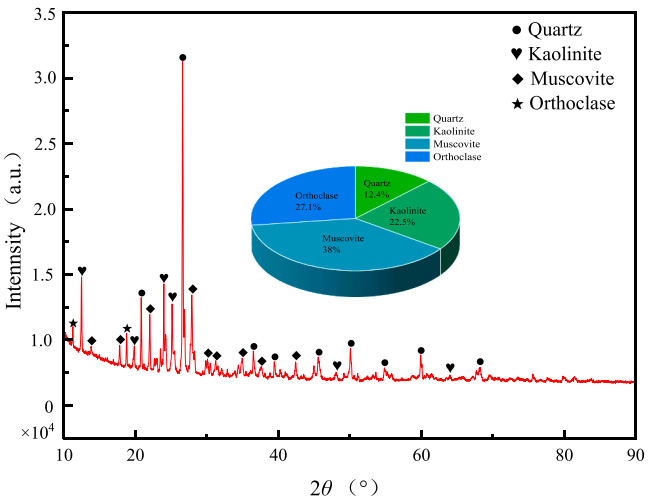

Fig. 2. XRD and XRF analyses of phyllite.

Table 2
Summary of chemical composition of the phyllite sample using XRF.

SiO_2	Al_2O_3	Fe_2O_3	K_2O	MgO	Na_2O
59.0	24.1	4.85	4.67	2.91	2.70

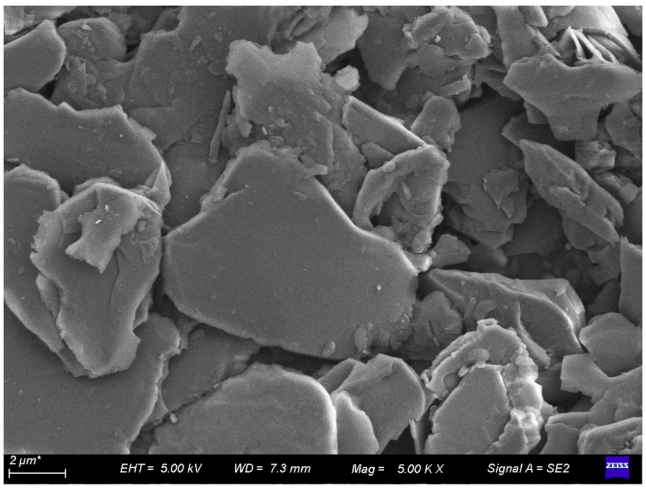

Fig. 3. SEM micrograph of a phyllite sample.

Table 3
Physical properties of weathered phyllite sample.

Moisture content (%)	Bulk density (g/cm^3)	Liquid limit (%)	Plastic limit (%)	Plasticity index
3–6.7	2.71–2.83	18.4	15.2	3.2

Point-load tests were conducted on weathered phyllite gravels using a point-load testing machine in accordance with the guidelines set by the International Society for Rock Mechanics (ISRM) [64]. The point-load strength index (P_{LI}) value was determined using the method described by Singh et al. [65]. The P_{LI} of weathered phyllite ranges between 0.94 and 6 MPa, with an average of 3.39 MPa. Consequently, the weathered phyllite gravels is classified as a type of soft rock [22,40,66].

2.2. Sample preparation

The primary aim of this study was to investigate the influence of GC on WPF. Coarse phyllite gravels were sorted by using the

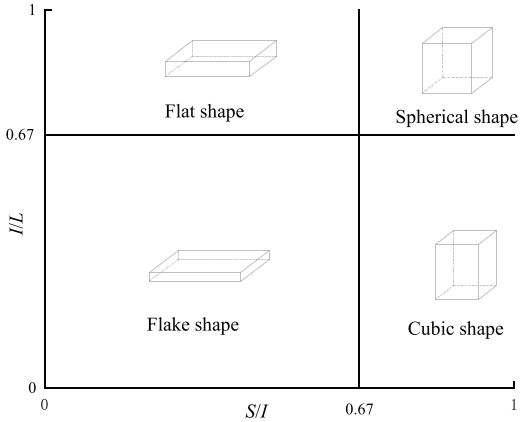

Fig. 4. Particle shape classification.

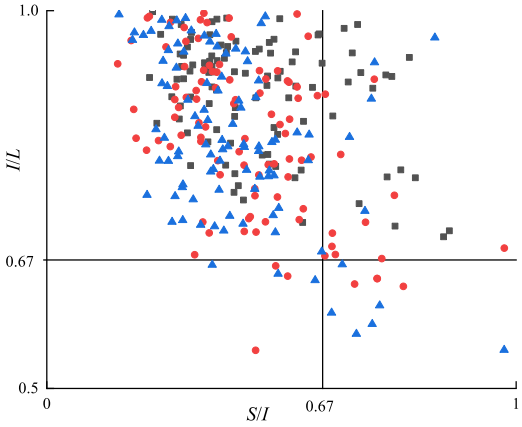

Fig. 5. Particle classification statistics.

following sieve sizes (mm): 60, 40, 20, 10, 5, 2, 1, 0.5, 0.25, and 0.075. Thus, the particle sizes ranging from 40–20, 20–10, 10–5, 5–2, 2–1, 1–0.5, 0.5–0.25, and 0.25–0.075 mm with a maximum particle size limit of 40 mm, as shown in Fig. 6.

Different GC weight percentages (30 %, 40 %, 50 %, 55 %, 60 %, and 70 %) were incorporated into the WPF samples for analysis. The PSD analysis for each WPF sample group were conducted following the ASTM C136/C136M-19 standard [67].

For any sample with a specific GC, the PSD curve can take on numerous forms, significantly influencing the physical and mechanical properties of the WPF. This experiment focuses on the effect of GC on WPF. To eliminate the interference caused by particle gradation, the particle gradation of gravel larger than 5 mm is fixed, as is the gradation of fine-grained soil smaller than 5 mm. Only the mass ratio of coarse and fine particles is used to determine the mass fraction of coarse particles. Using this method, the gradation curves of six groups of WPF samples with different GCs were designed, as illustrated in Fig. 7.

The gradation curve of WPF with 70 % GC is depicted at the lower end of Fig. 7., while that of WPF with 30 % GC is depicted at the upper end. Fig. 7. demonstrates a direct correlation between the GC percentage and particle coarseness in WPF. Furthermore, most groups exhibited coefficients of uniformity (C_u) exceeding 10 and coefficients of curvature (C_c) ranging from 1 to 2, indicating a well-graded nature across all WPF groups. Notably, among these groups, WPF with 55 % GC exhibited the highest C_u value and displayed a

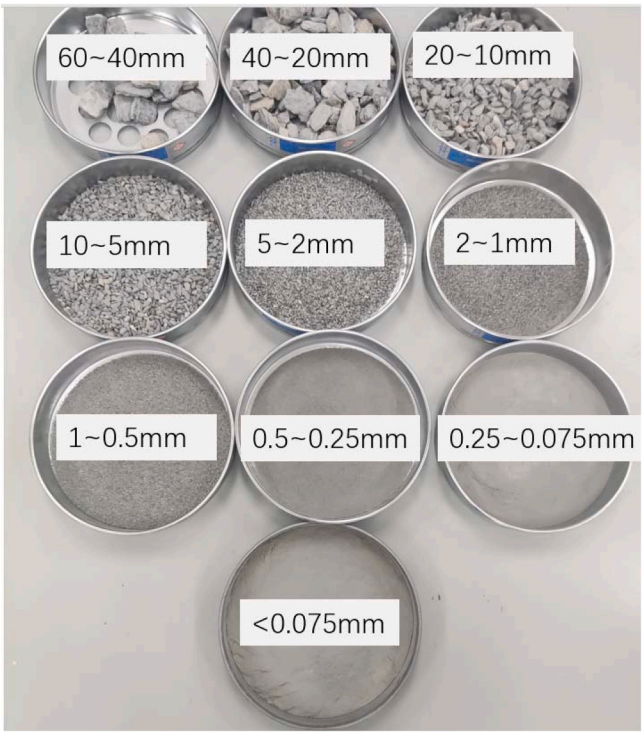

Fig. 6. Various weathered phyllite particle sizes.

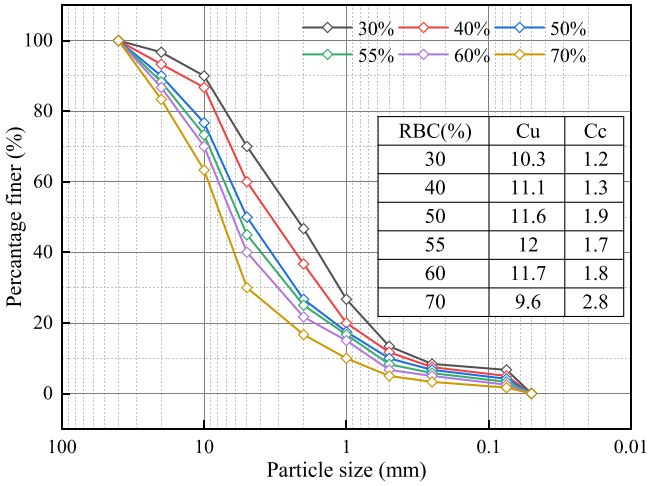

Fig. 7. Particle size distributions for weathered phyllite filler.

broader particle distribution compared to other groups.

The mold with 100 mm diameter and 200 mm height were selected to prepare standard cylindrical specimens for UCS test. The mold with 50 mm diameter and 50 mm height were selected to prepare cylindrical specimens for disintegration and penetration test. The WPF was loaded into the mold in three layers. After each layer was loaded, the surface was scraped and then the next layer was loaded. The finished mold was placed under the press, and the samples with different GC under the same compaction degree were prepared by static pressure method, and the sample preparation process is shown in Fig. 8.

2.3. Methods

2.3.1. Standard test for laboratory compaction

The aim of the standard test for laboratory compaction was to determine the maximum dry unit density (ρ_{dmax}) and optimum moisture content (w_{opt}), as well as to investigate the behavior of WPF during roadbed compaction. An electric compaction tester consisting of a rammer, controller, and cylindrical mold in accordance with ASTM D1557 [68] was used as the main apparatus (Fig. 9). Each 6-kg sample was divided into three layers for compaction, receiving 56 strikes per layer at a controlled compaction power of 2680 kJ. Five groups were established with varying moisture content: 2 %, 4 %, 6 %, 8 %, and 10 %. Water was added to the samples, which were then placed in plastic bags to maintain a constant water content over a period of 48 h. Following the completion of the compaction test, the samples were dried in an oven at temperatures reaching up to110 °C for at least 24 h before undergoing screening analysis to determine their PSD.

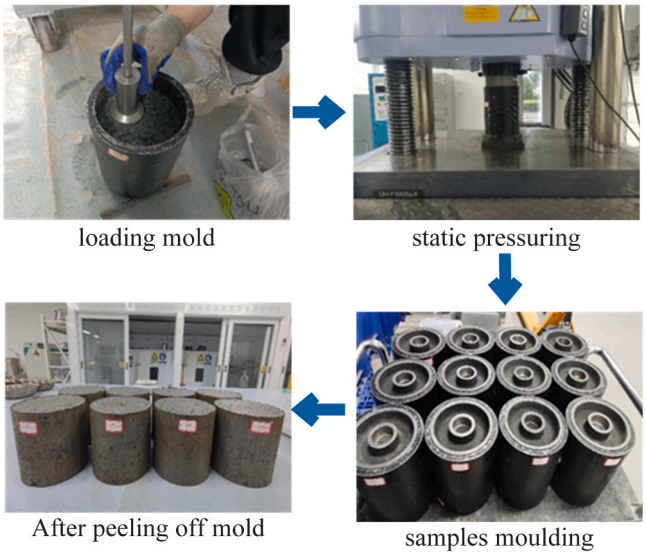

Fig. 8. Samples preparation process.

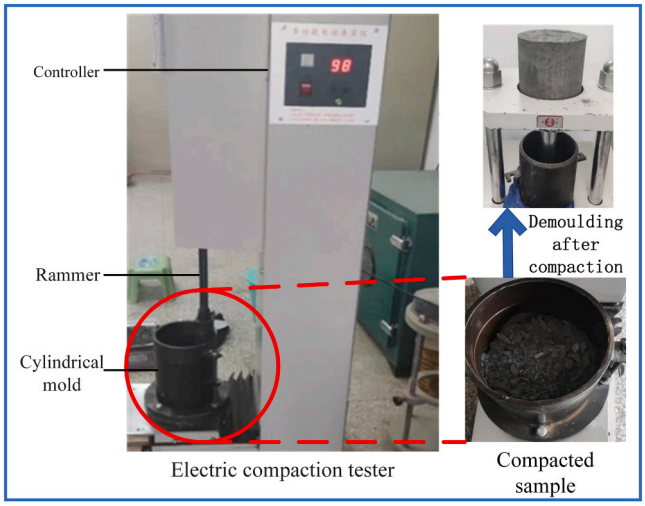

Fig. 9. Testing apparatus for compaction test.

2.3.2. *Unconfined compression test*

Unconfined compressive tests were conducted in accordance with ASTM D2166M-16 [69] to evaluate the UCS of WPF. An electric universal testing machine was used for specimen testing, as shown in Fig. 10. The samples were prepared at ρ_{dmax} and w_{opt} for different GCs. Cylindrical specimens 100 mm in diameter and 200 mm in height were used for the experiments. Loading was applied at a rate of 1 mm/min until failure. Three parallel tests were performed for each experimental condition and the average value was considered as the final result [70].

2.3.3. *California bearing ratio*

Following the Test Methods of Soils for Highway Engineering (JTG3430–2020) [71] and ASTM D1883–16 [72], the CBR samples were compacted at w_{opt} using three compaction hits (56 blows). Subsequently, the compacted samples were soaked to determine the CBR of the roadbed under extreme weather conditions. Following a soaking period of 96 h, as shown in Fig. 11, penetration tests were conducted on the samples with a surcharge weight of 5 kg applied during soaking. The top of the perforated plate was equipped with a dial indicator to measure the swelling properties of the samples during soaking. The CBR test machine featured a metallic grid plate and a tripod to securely hold the gauge on the mold. The hydraulic jack of the CBR test machine was used to apply a uniform pressure of 44.5 kN to the soil specimens at a loading rate of 1.27 mm/min. The load cell measures the magnitude of the force exerted by the piston penetration into the soil specimen.

The relationship between loads and penetration was visually represented through a graph, enabling the observation of both the CBR value and the load required for a 12.5-mm penetration. The corresponding CBR values for 2.5- and 5.0-mm penetrations were derived from this graphical representation using Eqs. (1a) and (1b) [73].

$$CBR_{2.5},\% = \frac{P_1}{7000} \times 100 \tag{1a}$$

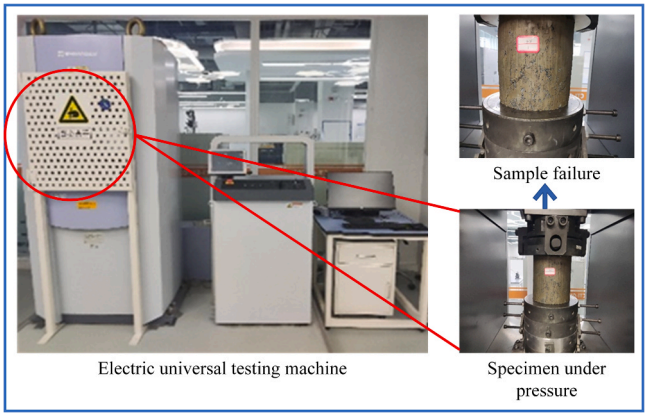

Fig. 10. Testing apparatus for UCS.

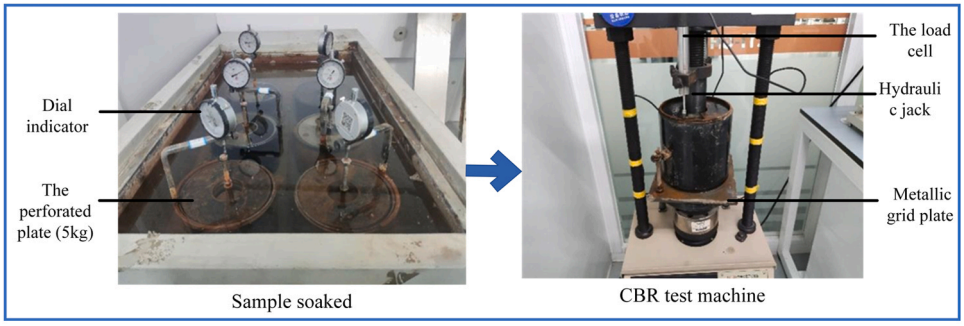

Fig. 11. CBR test.

$$CBR_{5.0}, \% = \frac{P_2}{10500} \times 100 \tag{1b}$$

Where: P_1 is the unit pressure at penetration of 2.5 mm; P_2 is the unit pressure at penetration of 5.0 mm.

2.3.4. *Penetration test*

The permeameter depicted in Fig. 12 features a flexible wall and was used for the penetration test. The test parameters were configured using a computer system, and control over the test was exerted using top, bottom, and confining pressure controllers. These controllers administer seepage confining pressure and back pressure to the sample. When the desired seepage pressure was reached, the computer control system automatically recorded the pertinent test parameters and computed the permeability coefficient of the sample based on Darcy's law.

2.3.5. *Disintegration test*

The disintegration test was performed using a disintegration testing device, as illustrated in Fig. 13, and the mass method was employed to assess the disintegration characteristics of the WPF. A cylindrical WPF sample 5 cm in height and 5 cm in diameter was gently positioned on a metal wire mesh and submerged in deionized water within a cylindrical plastic container. As the disintegration progressed, gradual fragmentation of the sample occurred, leading to the detachment and deposition of certain WPF particles into the plastic container. Consequently, this resulted in a reduction in the mass reading on the balance, which was subsequently utilized to calculate the rate of disintegration at each time point according to Eq. (2) [51,74,75]. Three samples were simultaneously tested under each experimental condition, and their average value was used as the final outcome.

$$K = \frac{m_0 - m_t}{m_0 - m_1} \times 100\% \tag{2}$$

Where: K is the disintegration ratio; m_0 is the initial balance reading at the commencement of the disintegration test; m_t is the balance reading at the time note t; m_1 is the balance reading when immersing an empty wire mesh into water.

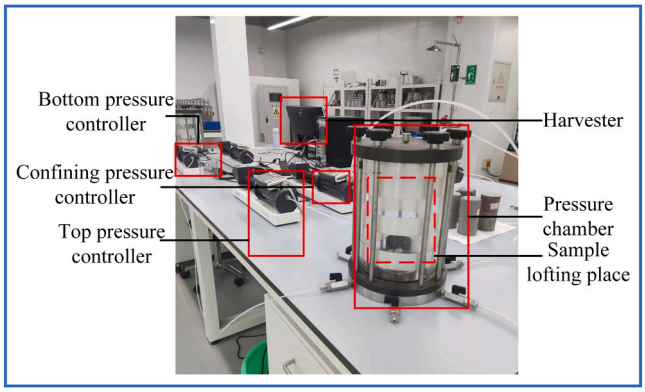

Fig. 12. Testing apparatus for penetration.

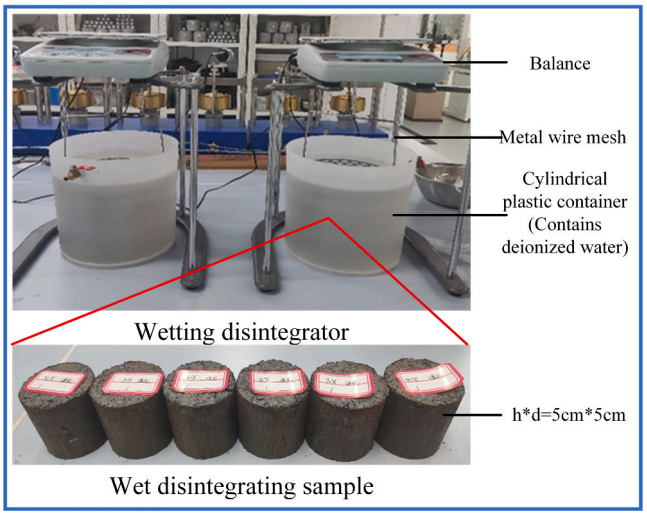

Fig. 13. Disintegration test.

3. Results and discussion

3.1. Compaction properties

The ρ_{dmax} and w_{opt} of the five WPF groups are shown in Fig. 14. ρ_{dmax} peaked at approximately 50 %–60 % GC, with corresponding values of 2.32 and 2.34 g/cm^3, while the respective w_{opt} were 5.82 % and 5.31 %. Within a GC range of 30 %–55 %, the phyllite gravels floated discretely in the WPF samples because of the presence of a large number of fine phyllite grains. During compaction, the phyllite gravels break, resulting in an increase in dry density. However, within a GC range of 50 %–60 %, the floating phyllite gravels transformed into framework-forming structures as an ample amount of fine phyllite grains filled the voids, creating a skeleton-dense structure that contributed to an increase in dry density. For specimens with GC exceeding 60 %, the WPF samples were transformed into highly fragmented rock mass mixtures comprising angular phyllite gravels and unoccupied voids. w_{opt} exhibited a declining trend as the GC increased. This decline can be attributed to the fact that fine grains possess greater water adsorption capacity than GC during compaction.

Based on the WPF compaction test results, the samples exhibited a maximum dry density upon compaction at approximately 50 %–60 % GC. Consequently, three groups were selected for parallel testing, with GC levels set at 40 %, 55 %, and 70 %. Water was added to the samples in accordance with w_{opt}. Initial compaction was performed for each group, and the quality of the phyllite with varying particle sizes was screened and documented. Subsequently, the samples were re-compacted using the same procedure and equipment.

The PSD of the WPF samples before and after compaction are shown in Fig. 15. Initially, the WPF gradation curve was positioned at the lower end, while the first and second gradation curves were located in the middle and upper positions, respectively. After

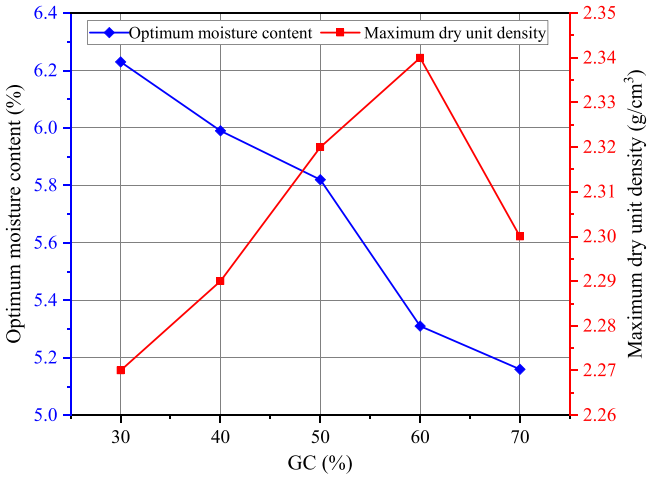

Fig. 14. Variation of ρ_{dmax} and w_{opt} with GCs.

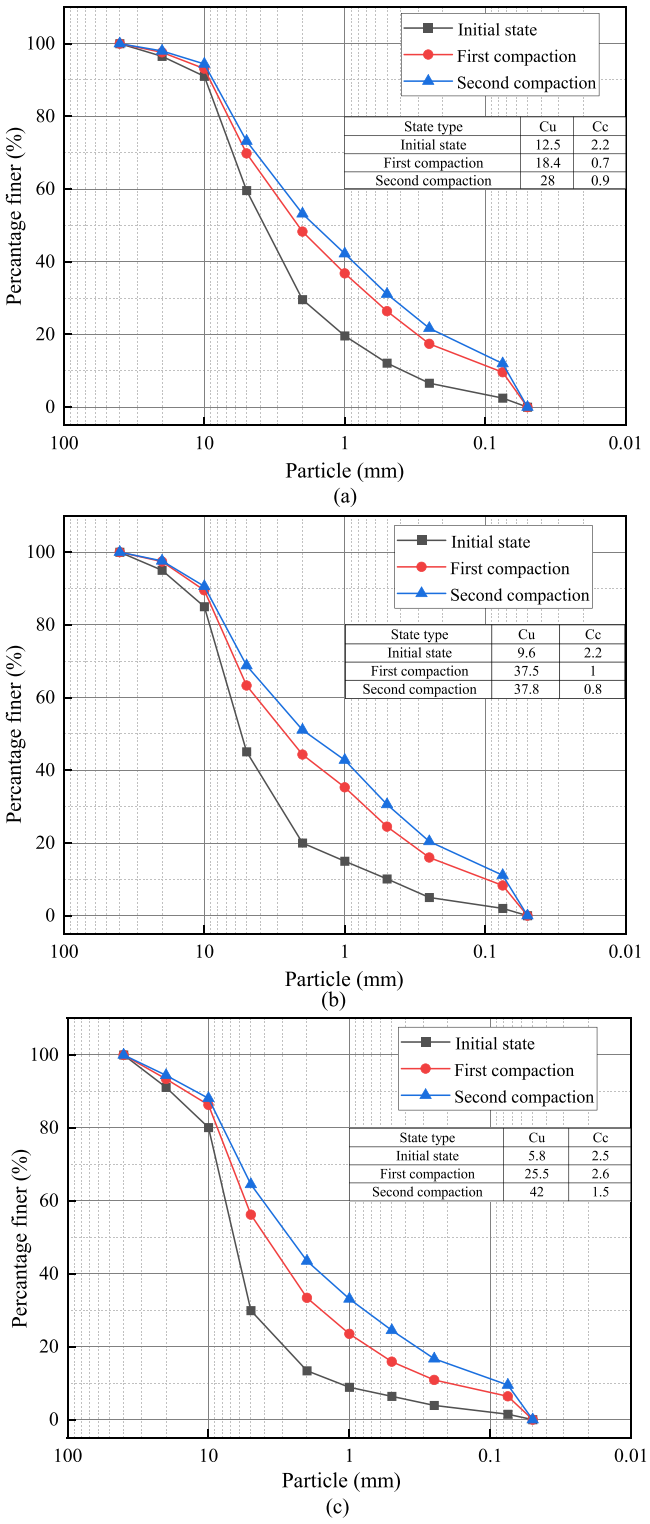

Fig. 15. Particle size distributions for the WPF before and after compaction. (a) GC= 40 %; (b) GC= 55 %; (c) GC= 70 %.

compaction, the PSD of the WPF samples became wider than in their initial states, accompanied by an increase in C_u. According to Hardin's definition of particle breakage [76], relative breakage (B_r) can be expressed mathematically as follows:

$$B_r = B_t / B_p \tag{3}$$

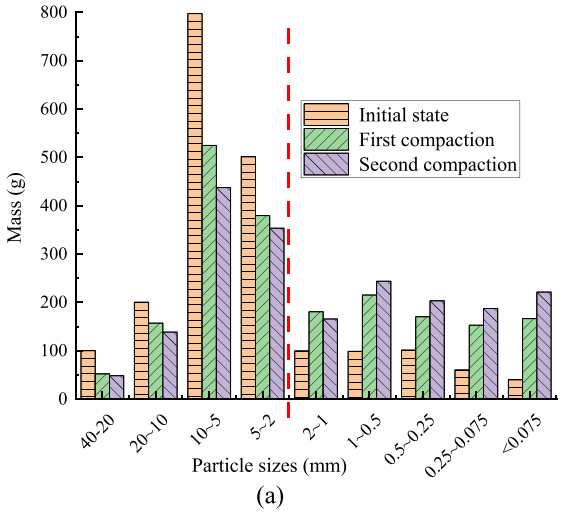

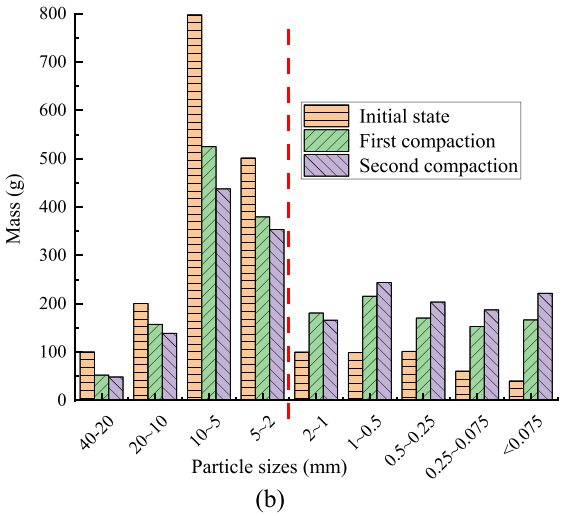

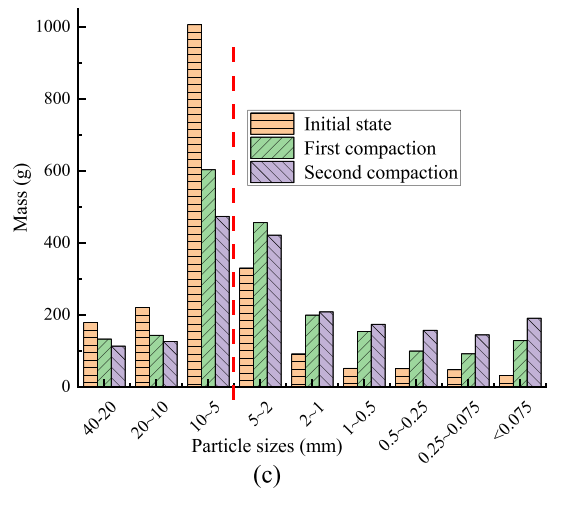

Fig. 16. Mass of WPF retained on various sieves before and after compaction: (a) GC= 40 %; (b) GC= 55 %; (c) GC= 70 %.

B_t represents the area enclosed by the gradation curve before and after compaction, as well as the vertical line at d= 0.075 mm; B_p denotes the area enclosed by the initial state's gradation curve and the vertical line at d= 0.075 mm.

The B_r values were determined at 40 %, 55 %, and 70 % GC to assess the extent of relative breakage in coarse phyllite gravels. After the first compaction, the average B_{r1} values were recorded as 24.2 %, 31.0 %, and 27.9 % respectively. Subsequently, after the second compaction, the average B_{r2} values increased to 32.7 %, 39.0 %, and 38.7 %, respectively. These findings indicate that compaction led to the fragmentation of coarse phyllite gravels, with an increase in GC resulting in a higher proportion of coarse phyllite gravels, as well as an elevated number and degree of particle breakage during the first and second compactions. The WPF experienced further fragmentation during the second compaction than during the first. B_{r1} and B_{r2} reached their maximum at 55 % GC, providing insight into the underlying cause of the highest observed dry density at this GC. Coarse phyllite gravels break into finer grains, effectively filling all interstitial voids between particles of varying sizes, resulting in a higher concentration of phyllite particles per unit volume. Consequently, the samples exhibited enhanced densification, leading to improved mechanical and hydraulic properties (as supported by the subsequent analysis of these properties).

The mass of the WPF grains varied with the compaction effort, as shown in Fig. 16. Specifically, the mass of particles larger than 2 mm exhibited a decreasing trend, while the mass of particles smaller than 2 mm increased with 40 % and 55 % GC. In comparison to the initial state samples, after the first and second compactions, there was a reduction in the mass of coarse phyllite gravels (>5 mm) by 24.4 % and 32.9 % for 40 % GC respectively; by 33.1 % and 43.1 % for 55 % GC, respectively; and by 37.5 % and 49.4 % for 70 % GC, respectively. The term "compaction effort" refers to the total energy input applied to the particles [40]. During compaction, the mass of the coarse phyllite gravels decreased, while that of fine grains increased. This observation suggests that compaction leads to the fragmentation of coarse gravels into fine grains. The underlying reason for this phenomenon lies in the higher strength exhibited by fine grains compared to larger ones [77–79]. Previous studies also reported an increase in the mass of fine grains with an increase in GC [80–83]. These findings imply that both the compaction effort and initial GC of the WPF influenced the extent of particle breakage.

3.2. Mechanical properties

3.2.1. Unconfined compression strength

The UCS is utilized for assessing the effectiveness and significance of various factors influencing the roadbed's strength [84]. Previous studies have indicated that when the GC ranges from 20 % to 70 %, both rock blocks and fine grains exert control over the UCS of SRM [41,42,45,85]. GC exhibits positive and negative effects on the UCS [43].

The strength of the WPF is determined by the synergy between the gravels, fine grains, and gravel-soil interface interactions. As shown in Fig. 17 and Fig. 18, in low-GC cases (30 %–50 %), angularity and strength provided by phyllite gravels contribute to the overall WPF friction, resulting in an increase in UCS. The increase in gravels replaced the fine grains, leading to a decrease in cohesion; however, this decrease was outweighed by an increase in friction. For 55 % GC, the maximum UCS was 257 kPa. Phyllite gravels contact each other to form a skeleton, and fine grains fill the skeleton to create a dense structure. Additionally, the coarse gravels possess abundant edges and corners that enhance block interlocking and the internal friction angle. Consequently, both coarse and fine grains synergistically resist external loads, effectively mitigating the stress on larger particles. The decline occurred subsequent to the GC exceeding 55 %. Chen et al. [86] discovered that there exists a GC threshold, defined as 53 %–58.5 %, for restructuring the permeable granular framework; this finding was corroborated by Liu et al. [40]. This decrease can be attributed to the replacement of fine grains with phyllite gravels, which increases the number of soil-gravel contact surfaces and consequently weakens the connections between the fine grains and gravels, resulting in reduced cohesion. Furthermore, because of the scarcity of fine grains that fill the framework formed by the coarse gravels, these coarse gravels experience higher stress levels and are more prone to breakage [79,87]. The reduction in cohesion outweighs the increase in friction. Similar conclusions have been reported in previous studies [24,44,88].

3.2.2. California bearing ratio

CBR is a crucial parameter for assessing the bearing capacity and engineering properties of roadbed fillers under adverse conditions [89]. As shown in Fig. 19, all CBR values satisfy the specified threshold of 8 % for highways subjected to water immersion [90]. This indicates that the WPF exhibited a commendable roadbed-bearing capacity even after water immersion. Moreover, an increase in compactness while maintaining a constant GC leads to an increase in CBR. The CBR values were highest for the WPF with a GC of 55 %, reaching 25.92 %, 26.2 %, and 29.11 % at compactness degrees of 93 %, 94 %, and 96 %, respectively. At a compactness of 96 %, compared to GC at 40 % and 70 %, the CBR increased by approximately 10.17 % and 8.85 %, respectively. A reasonable GC can significantly enhance the bearing capacity of the WPF, while samples with 55 % GC exhibited stronger resistance to local deformation.

It has been experimentally confirmed that WPFs with a GC ranging from 50 %–60 % possess a more compact and robust structure, which aligns with previous findings indicating a critical GC threshold [91–93]. Zhao et al. [30] concluded that the critical threshold for SGM was set at 50 %. Similarly, Liu et al. [40] determined that the same critical threshold for WPF is established at 55 %. As the compactness degree increased, water absorption decreased. Notably, as shown in Fig. 20, samples with 55 % GC exhibited the lowest water absorption, indicating a decrease in internal voids that effectively prevented water infiltration. The compactness degree not only determines the CBR but also influences the water absorption of the WPF. Therefore, it is imperative to control the filler's compactness degree in engineering projects to enhance the strength and bearing capacity while minimizing water infiltration into the roadbed.

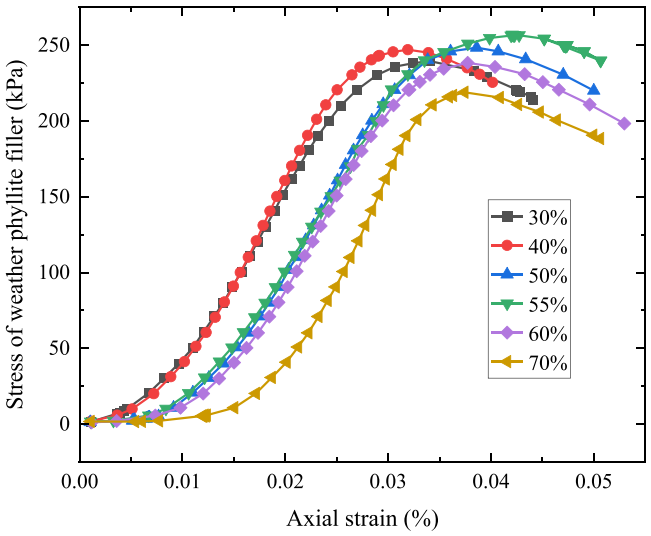

Fig. 17. UCS–axial strain curves of WPF.

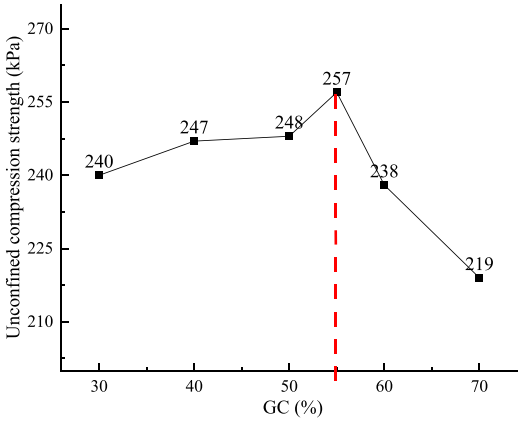

Fig. 18. Relationship between UCS and GCs.

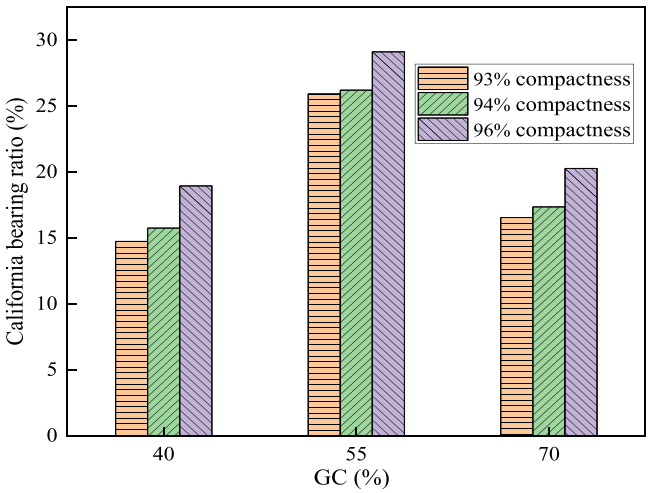

Fig. 19. Relationship between CBR and GCs.

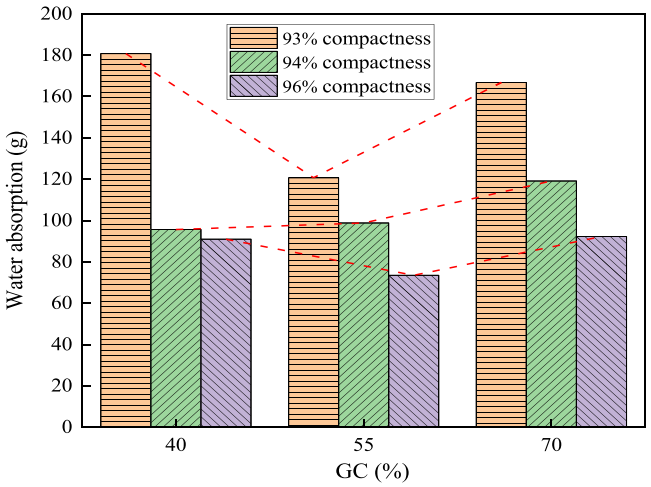

Fig. 20. Relationship between water absorption and GCs.

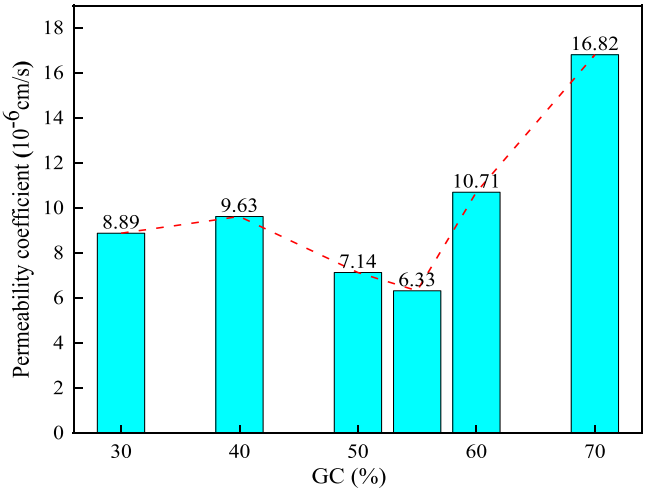

Fig. 21. Relationship between permeability coefficient and GCs.

3.3. Hydraulic properties

3.3.1. Permeability

Fig. 21 illustrates the relationship between the permeability coefficient and GC. The change in permeability coefficient for WPF samples with 30 %–60 % GC was negligible, all falling within a range of 10^{-6} cm/s. As the GC increased, the permeability coefficient decreased until it reached a minimum at 55 % GC. This can be attributed to the addition of fewer low-permeability phyllite gravels to the WPF as the GC increased, resulting in an increase in the void ratio of the fine-grained fraction [94]. The presence of phyllite gravels diluted the physicochemical potential of the WPF [52], resulting in a decrease in the permeability coefficient. When the GC exceeded 55 %, there was an increase in permeability. Beyond 70 % GC, the permeability coefficient exhibited a significant increase, more than ten-fold. It appears that insufficient fine grains were present within the WPF, and the macro voids developed between phyllite gravels were partially filled by these fine grains. This finding aligns with the observations regarding the compaction and strength characteristics.

It is commonly assumed that the permeability of a geomaterial mixture is controlled by the content and nature of the fine grains. Previous test results have indicated an increase in the permeability coefficient with an increase in GC [85]. However, the current test results for the WPF permeability coefficient with different GCs align with the findings of previous studies [48,94–97]. Shakoor and Cook [94] conducted tests on silty clay/gravel mixtures and observed a range of 1–2 $\times$ 10^{-7} cm/s for the permeability coefficient at GCs between 0 % and 50 %. Shelley and Daniel [95] concluded that for GCs below 60 %, the permeability coefficient of compacted soil/gravel mixtures was less than 1 $\times$ 10^{-7} cm/s. The permeability coefficient of residual soil-gravelly sand mixtures remained within a range of 10^{-7} cm/s up to the addition of 50 % gravelly sand, as indicated by Indrawan et al. [96]. Shafiee [97] and Wang et al. [48]

observed a turning point in the variation of the permeability coefficient with increasing GC, where the minimum permeability was achieved at 40 % GC. Zhao et al. [30] found that for WPF, the minimum permeability was attained at 50 % GC. Extensive experimental data from previous studies on SGMs have demonstrated that the permeability of SGM does not significantly increase until reaching a critical GC (60 %–75 %); beyond this threshold, there is a substantial increase in SGM permeability with further increases in GC [47,86,96,97].

The fine and coarse grains in the WPF both originate from the phyllite rock formation, and their properties are primarily influenced by the parent rock. They have identical mineral and chemical compositions. Due to the abundance of non-clay minerals (such as orthoclase and quartz) in phyllite rock, the WPF can be considered as a non-cohesive material, resulting in low plasticity for fine grains. Permeability is controlled by the void ratio when fine grains exhibit low plasticity [97]. The void ratio is closely associated with compaction, where samples achieve maximum dry density and minimum void ratio after compaction when the GC ranges between 50 % and 60 %.

3.3.2. Disintegration characteristics

The disintegration characteristics are used to evaluate the resistance of geomaterials to softening and disintegration upon contact with water [98]. The WPF disintegration ratio increased during the initial soaking stage, indicating that prolonged exposure to water accelerated the disintegration process. Disintegration occurred within approximately 10 min. Samples with 50 % and 55 % GC exhibited a maximum disintegration time of 10 and 11 min, respectively. Samples with 30 % and 60 % GC experienced a disintegration time of approximately 8 min. Thus, WPF displays limited resistance to disintegration and readily undergoes softening and fragmentation when exposed to water.

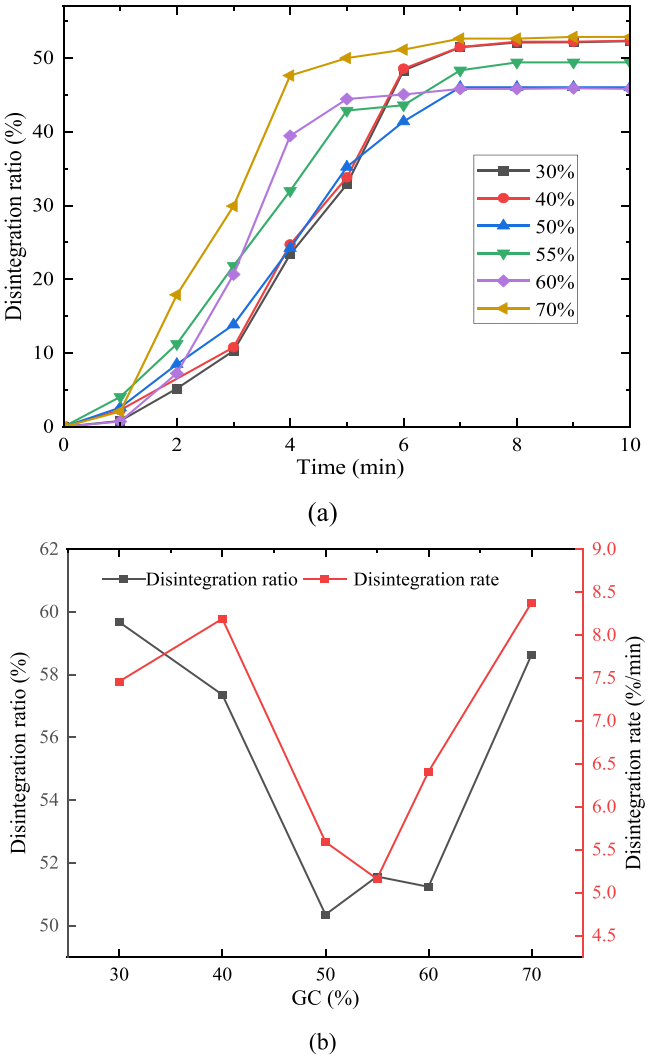

Fig. 22. Disintegrating curves of samples: (a) Variation of disintegration ratio with time. (b) Variation of disintegration ratio and disintegration rate with GCs.

The relationship between the disintegration rate and GC is shown in Fig. 22. For WPF samples with 30 %–70 % GC, there is no significant variation observed in the average disintegration rate, which ranges from 5.16 % to 8.38 %/min. Zhao et al. [29] reported a disintegration rate of phyllite soil of 10.0 %·min^{-1}, suggesting that the initial decrease followed by an increase in GC leads to changes in the disintegration rate. Notably, WPF samples with 50 %–60 % GC exhibited the lowest disintegration rate among all tested samples. The permeability behavior exhibited a similar trend. The disintegration of geomaterials is attributed to the swelling of clay minerals [99]. However, the XRD analysis did not detect smectite; only kaolinite (22.5 %) was identified, which exhibits limited water sensitivity. In the case of the investigated WPF in this study, it is reasonable to anticipate that compaction plays a crucial role in determining its disintegration behavior. As discussed previously, when the GC reaches 50 %–60 %, the samples became more compact and exhibited enhanced resistance against disintegration. A higher compaction degree leads to a more stable disintegration behavior [54,77].

4. Conclusion

The compaction, mechanical, and hydraulic properties of a WPF composed of coarse gravels and fine grains were comprehensively analyzed through a series of laboratory tests, including standard test for laboratory compaction, UCS, CBR, permeability, and disintegration tests. Based on the experimental results and analyses, the main conclusions of this study can be summarized as follows.

(1) The fine and coarse grains in the WPF both originate from the phyllite rock formation, and their properties are primarily influenced by the parent rock. Unlike phyllites in other areas, the XRD, XRF, and SEM analysis results revealed that the Longnan phyllite exhibits higher concentrations of muscovite and orthoclase, but relatively lower levels of quartz. Clay minerals consist exclusively of kaolinite, which has a limited water absorption capacity. Consequently, it can be inferred that the WPF can be classified as a non-cohesive material.

(2) The compaction properties of the WPF were examined, and the results revealed that the maximum dry unit density exhibited an initial increase followed by a subsequent decrease with varying GCs, reaching its peak at approximately 50 %–60 % GC. When the GC was below 50 %, discrete phyllite gravels were observed to float within the WPF samples. Within GC range of 50 %–60 %, these floating phyllite blocks underwent a transformation into framework-forming structures, as a substantial amount of fine phyllite grains effectively filled all interstitial voids between particles, resulting in a higher phyllite particle concentration per unit volume. At 55 % GC, under compaction effort, coarse phyllite gravels experienced increased breakage, leading to a broader particle distribution and higher values of both the relative breakage coefficient (B_r) and uniformity (C_c) compared to their initial state.

(3) The UCS results for the WPF indicate that in low-GC cases (30 %–50 %), the angularity and strength provided by phyllite gravels contribute to the overall WPF friction, resulting in an increase in UCS. For 55 % GC, the maximum UCS was recorded as 257 kPa. The coarse phyllite gravels possess abundant edges and corners that enhance block interlocking and the internal friction angle, synergistically resisting external loads along with fine grains, and effectively mitigating stress on larger particles. However, for GC above 55 %, the UCS values declined because of the replacement of fine grains with phyllite gravels, increasing soil-gravel contact surfaces, and consequently reducing cohesion. A similar pattern was observed in the CBR results; reaching its peak at 55 % GC and exhibiting stronger resistance to local deformation.

(4) The permeability and disintegration test results indicate that for WPF, its permeability coefficient ranges between 10^{-6} cm/s for GC up to 60 %. For a GC of less than 60 %, the presence of coarse phyllite gravels had a slight beneficial effect on reducing the WPF permeability coefficient. However, when the GC exceeds 70 %, there is a noticeable increase in the permeability coefficient. Similar trends can also be observed in the disintegration behavior; both phenomena are influenced by the void ratio when the fine grains have low plasticity. It should be noted that the void ratio is closely associated with compaction, indicating its significant role in determining the hydraulic characteristics. Notably, when the GC reached approximately 50 %–60 %, the samples demonstrated improved compactness and enhanced resistance against both permeation and disintegration. Higher compaction degrees lead to greater stability in the hydraulic behavior.

Based on the above, this study analyzes the compaction properties, mechanical properties, and hydraulic characteristics of WPF with different ratios of GC. A critical GC threshold for WPF is identified, indicating that within the GC range of 50–60 %, the phyllite gravels contact each other, forming a skeletal structure. Meanwhile, fine grains effectively fill the interstitial voids between particles, resulting in a higher concentration of phyllite particles per unit volume. At 55 % GC, the WPF exhibits optimal compaction, achieving the highest values for bulk density, compressive strength, C_u, B_r, UCS, and CBR, alongside the lowest permeability and disintegration rates.

List of abbreviations

Full name	Abbreviations
Waste rock block	WRB
Geotechnical properties tests	GPTs
Proctor compaction test	PCT

(*continued on next page*)

(*continued*)

Unconfined compressive strength	UCS
California bearing ratio	CBR
X-ray diffraction	XRD
X-ray fluorescence	XRF
Mercury intrusion porosimetry	MIP
Scanning electron microscope	SEM
Soil and gravel mixture	SGM
Gravel content	GC
Weathered phyllite filler	WPF
American Society for Testing Materials	ASTM
International Society for Rock Mechanics	ISRM
Point-load strength index	P_{LI}
Particle size distribution	PSD
Coefficients of uniformity	C_u
Coefficients of curvature	C_c
Maximum dry unit density	ρ_{dmax}
Optimum moisture content	w_{opt}
Relative breakage	B_r

CRediT authorship contribution statement

Zhang Yanjie: Writing – original draft. **Lai Weizhong:** Data curation. **Wang Xu:** Supervision. **Zhu Hanxing:** Writing – review & editing. **An Liang:** Investigation.

Declaration of Competing Interest

The authors declare that they have no known competing financial interests or personal relationships that could have appeared to influence the work reported in this paper.

Acknowledgements

This work was supported the National Natural Science Foundation of China (Grant Nos. 52268058; W2421075); Tianyou Youth Talent Lift Program of Lanzhou Jiaotong University; Key research and development project of Lanzhou Jiaotong University (LZJTU-ZDYF2305); Gansu Provincial Department of Education Industrial Support Program Project, China (2023CYZC-34); Gansu Provincial Science and Technology Major Special Project (21ZD3GA002);

Data Availability

Data will be made available on request.

References

[1] A. Arulrajah, M.M.Y. Ali, J. Piratheepan, M.W. Bo, Geotechnical properties of waste excavation rock in pavement subbase applications. J. Mater. Civil. Eng. 24 (7) (2012) 924–932, https://doi.org/10.1061/(ASCE)MT.1943-5533.0000419.
[2] A. Arulrajah, A. Mohammadinia, A. D'Amico, S. Horpibulsuk, Effect of lime kiln dust as an alternative binder in the stabilization of construction and demolition materials, Constr. Build. Mater. 152 (2017) 999–1007, https://doi.org/10.1016/j.conbuildmat.2017.07.070.
[3] M.A. Al-Obaydi, M.D. Abdulnafaa, O.A. Atasoy, A.F. Cabalar, Improvement in field CBR values of subgrade soil using construction-demolition materials, Transp. Infrastruct. Geotech. 9 (2022) 185–205, https://doi.org/10.1007/s40515-021-00170-x.
[4] A.F. Cabalar, M.D. Abdulnafaa, V. Isbuga, Plate loading tests on clay with construction and demolition materials, Arab. J. Sci. Eng. 46 (2021) 4307–4317, https://doi.org/10.1007/s13369-020-04916-6.
[5] P. Segui, A. e M. Safhi, M. Amrani, M. Benzaazoua, Mining wastes as road construction material: a review, Minerals 13 (90) (2023), https://doi.org/10.3390/min13010090.
[6] F. Maghool, A. Arulrajah, Y.J. Du, S. Horpibulsuk, A. Chinkulkijniwat, Environmental impacts of utilizing waste steel slag aggregates as recycled road construction materials, Clean. Tech. Environ. Policy 19 (4) (2017), https://doi.org/10.1007/s10098-016-1289-6.
[7] M. Amrani, Y. Taha, A. Elghali, M. Benzaazoua, A. Kchikach, R. Hakkou, An experimental investigation on collapsible behavior of dry compacted phosphate mine waste rock in road embankment, Transp. Geotech. 26 (2021) 100439, https://doi.org/10.1016/j.trgeo.2020.100439.
[8] A.F. Cabalar, S.O. Alosman, Influence of rock powder on the behaviour of an organic soil, Bull. Eng. Geol. Environ. 80 (2021) 8665–8676, https://doi.org/10.1007/s10064-021-02457-2.
[9] A.F. Cabalar, R.A. Omar, Stabilizing a silt using waste limestone powder, Bull. Eng. Geol. Environ. 82 (2023) 300, https://doi.org/10.1007/s10064-023-03302-4.
[10] N. Bella, M.A. Dahane, T.A. Mebarki, A. Benmalek, M. Benallal, Valorisation of coal mine tailings in roads construction. Alger. J. Environ. Sci. Technol. 8 (2022) 2307–2313.
[11] A.F. Cabalar, S.O. Hama, S. Demir, Behaviour of a clay and gravel mixture, Balt. J. Road. Bridge Eng. 17 (1) (2022) 98–116, https://doi.org/10.7250/bjrbe.2022-17.553.
[12] A. Mishra, S.K. Das, K.R. Reddy, Characterization and environmental sustainability of open pit coal mine overburden waste rock as pavement geomaterial, Transp. Geotech. 42 (2023) 101094, https://doi.org/10.1016/j.trgeo.2023.101094.

[13] J. Kostrzewa, P. Popielski, A. Dabska, Geotechnical properties of washed mineral waste from grit chambers and its potential use as soil backfill and road embankment materials, Buildings 14 (2024) 766, https://doi.org/10.3390/buildings14030766.
[14] R.K. Etim, A.O. Eberemu, K.J. Osinubi, Stabilization of black cotton soil with lime and iron ore tailings admixture, Transp. Geotech. 10 (2017) 85–95, https://doi.org/10.1016/j.trgeo.2017.01.002.
[15] N.C. Consoli, A.P. Silva, H.P. Nierwinski, J. Sosnoski, Durability, strength, and stiffness of compacted gold tailings - cement mixes, *Can. Geotech. J.* 55 (4) (2018) 486–494, https://doi.org/10.1139/cgj-2016-0391.
[16] M. Amrani, Y. Taha, A. Kchikach, M. Benzaazoua, R. Hakkou, Phosphogypsum recycling: New horizons for a more sustainable road material application], J. Build. Eng. 30 (2020) 101267, https://doi.org/10.1016/j.jobe.2020.101267.
[17] V. Shanmugasundaram, B. Shanmugam, Application of cement treated magnesite mine tailings as subgrade, Constr. Build. Mater. 365 (2023) 130064, https://doi.org/10.1016/j.conbuildmat.2022.130064.
[18] L. Manjarrez, L. Zhang, Utilization of copper mine tailings as road base construction material through geopolymerization, J. Mater. Civ. Eng. 2 (30) (2018) 04018201, https://doi.org/10.1061/(ASCE)MT.1943-5533.0002397.
[19] M. Amrani, Y. El Haloui, P. Hajikarimi, H. Sehaqui, R. Hakkou, M. Barbachi, Y. Taha, Feasibility of using phosphate wastes for enhancing high-temperature rheological characteristics of asphalt binder, J. Mater. Cycles Waste Manag 22 (2020) 1407–1417, https://doi.org/10.1007/s10163-020-01026-1.
[20] Y. Li, Y. Zhang, J. Bi, Y. Zhao, Y. Li, X. Zhong, K. Zheng, Influences of calcium and magnesium sources on microbially modified strongly weathered phyllite filler, Constr. Build. Mater. 416 (2024) 135118, https://doi.org/10.1016/j.conbuildmat.2024.135118.
[21] X.S. Zhao, Z.T. Fu, Q.J. Yang, K. Yao, D.X. Geng, K. Li, Subgrade fill strength and bearing characteristics of weathered phyllite blended with red clay, Road. Mater. Pavement 22 (11) (2020) 2571–2590, https://doi.org/10.1080/14680629.2020.1773906.
[22] X.S. Mao, C.J. Miller, L.Q. Liu, Cement improved highly weathered phyllite for highway roadbeds: a case study in Shaanxi province, J. Traffic Transp. Eng. -Engl. Ed. 4 (4) (2017) 403–411, https://doi.org/10.1016/j.jtte.2017.07.003.
[23] A.F. Cabalar, I.A. Ismael, A. Yavuz, Use of zinc coated steel CNC milling waste for road pavement subgrade, Transp. Geotech. 23 (2020) 100342, https://doi.org/10.1016/j.trgeo.2020.100342.
[24] L. Feng, W. Liu, W. Jiang, G. Wang, Mechanics and road performance of mudstone modified stabilized gravel subgrade in arid desert areas, Case Stud. Constr. Mat. 20 (2024) e02799, https://doi.org/10.1016/j.cscm.2023.e02799.
[25] X. Luo, Z. Lu, H. Yao, J. Zhang, W. Song, Experimental study on soft rock subgrade reinforced with geocell, Road. Mater. Pavement 23 (9) (2022) 2190–2204, https://doi.org/10.1080/14680629.2021.1948907.
[26] X. Wang, G. Yang, F. Tan, Y. Lin, B. Zhai, The performance of construction waste backfilling subway depot—A case study in Zhengzhou, Case Stud. Constr. Mat. 18 (2023) e01900, https://doi.org/10.1016/j.cscm.2023.e01900.
[27] Y.J. Zhang, X. Wang, Y.X. Yin, L. Zhao, Experimental study on railway subgrade filling material of phyllite spoil improved with cement, J. China Railw. Soc. 36 (6) (2014) 81–86, https://doi.org/10.3969/j.issn.1001-8360.2014.06.013.
[28] T.S. Valera, A.P. Ribeiro, F.R. Valenzuela-Díaz, A. Yoshiga, W. Ormanji, S.M. Toffoll, The effect of phyllite as a filler for PVC plastisols San Francisco, in: Proceedings of the 60th Annual 379 Technical Conference of the Society of Plastics Engineers, USA, (2002) 3949-3953.
[29] X. Zhao, L. Zhao, Q. Yang, Z. Wang, A. Cheng, L. Mo, J. Yan, Permeability and disintegration characteristics of composite improved phyllite soil by red clay and cement, Minerals 13 (1) (2023) 32, https://doi.org/10.3390/min13010032.
[30] Y. Zhao, Y. Li, C. Wang, K. Xue, G. Chen, P. Liu, Road performance of ordinary Portland cement improvement of strongly weathered phyllite filler, Constr. Build. Mater. 350 (2022) 128801, https://doi.org/10.1016/j.conbuildmat.2022.128801.
[31] C. Arce, E. Garzón, P.J. Sánchez-Soto, Phyllite clays as raw materials replacing cement in mortars: Properties of new impermeabilizing mortars, Constr. Build. Mater. 224 (2019) 348–358, https://doi.org/10.1016/j.conbuildmat.2019.07.081.
[32] E. Garzón, M. Cano, B.C. OKelly, P.J. Sánchez-Soto, Effect of lime on stabilization of phyllite clays, Appl. Clay Sci. 123 (2016) 329–334, https://doi.org/10.1016/j.clay.2016.01.042.
[33] N. Mohamad, K. Muthusamy, R. Embong, A. Kusbiantoro, M.H. Hashim, Environmental impact of cement production and solutions: a review, Mater. Today.: Proc. 48 (2022) 741–746, https://doi.org/10.1016/j.matpr.2021.02.212.
[34] H.X. Chen, X.W. Ma, H.J. Dai, Reuse of water purification sludge as raw material in cement production, Cem. Concr. Compos. 32 (6) (2010) 436–439, https://doi.org/10.1016/j.cemconcomp.2010.02.009.
[35] D. Feng, Y. Wang, D. Chen, S. Liang, Experimental study on the influence mechanism of clay particles on the microbial treatment of granite residual soil, Constr. Build. Mater. 411 (2024) 134659, https://doi.org/10.1016/j.conbuildmat.2023.134659.
[36] S. Sabine, The role of universities in fostering sustainable development at the regional level, J. Clean. Prod. 48 (2013) 74–84, https://doi.org/10.1016/j.jclepro.2013.01.029.
[37] W. Xu, J. Xu, J. Liu, H. Li, B. Cao, X. Huang, G. Li, The utilization of lime-dried sludge as resource for producing cement, J. Clean. Prod. 83 (2014) 286–293, https://doi.org/10.1016/j.jclepro.2014.07.070.
[38] D. Cen, D. Huang, F. Ren, Shear deformation and strength of the interphase between the soil-rock mixture and the benched bedrock slope surface, Acta Geotech. 12 (2017) 391–413, https://doi.org/10.1007/s11440-016-0468-2.
[39] R.L. Hu, X. Li, Y. Wang, W. Gao, J.G. Xia, Z.Q. Li, W.W. Gao, Y.S. Sun, Research on engineering geomechanics and structural effect of soil-rock mixture, J. Eng. Geol. 28 (2) (2020) 255–281. ⟨http://www.gcdz.org/article/doi/10.13544/j.cnki.jeg.2020-077⟩.
[40] F. Liu, X. Mao, Y. Fan, L. Wu, W.V. Liu, Effects of initial particle gradation and rock content on crushing behaviors of weathered phyllite fills–A case of eastern Ankang section of Shiyan–Tianshui highway, China, J. Rock. Mech. Geotech. Eng. 12 (2) (2020) 269–278, https://doi.org/10.1016/j.jrmge.2019.07.011.
[41] E.S. Lindquist, The Strength and Deformation Properties of Melange, University of California, Berkeley, 1994.
[42] L.E. Vallejo, R. Mawby, Porosity influence on the shear strength of granular material-clay mixtures, Eng. Geol. 58 (2) (2000) 125–136, https://doi.org/10.1016/S0013-7952(00)00051-X.
[43] Z. Zhang, Q. Sheng, X. Fu, Y. Zhou, J. Huang, Y. Du, An approach to predicting the shear strength of soil-rock mixture based on rock block proportion, Bull. Eng. Geol. Environ. 79 (2020) 2423–2437, https://doi.org/10.1007/s10064-019-01658-0.
[44] W.J. Xu, Z.Q. Yue, R.L. Hu, Study on the mesostructure and mesomechanical characteristics of the soil-rock mixture using digital image processing based finite element method, Int. J. Rock. Mech. Min. 45 (5) (2008) 749–762, https://doi.org/10.1016/j.ijrmms.2007.09.003.
[45] S. Wang, Y. Li, X. Gao, Q. Xue, P. Zhang, Z. Wu, Influence of volumetric block proportion on mechanical properties of virtual soil-rock mixtures, Eng. Geol. 278 (2020) 105850, https://doi.org/10.1016/j.enggeo.2020.105850.
[46] L.E. Vallejo, Interpretation of the limits in shear strength in binary granular mixtures, Can. Geotech. J. 38 (5) (2001) 1097–1104, https://doi.org/10.1139/t01-029.
[47] W. Gao, R.L. Hu, I.A. Oyediran, Z.Q. Li, X.Y. Zhang, Geomechanical characterization of Zhangmu soil-rock mixture deposit, Geotech. Geo. l Eng. 32 (2014) 1329–1338, https://doi.org/10.1007/s10706-014-9808-x.
[48] Y. Wang, X. Li, B. Zheng, S.D. Li, Y.T. Duan, A laboratory study of the effect of confining pressure on permeable property in soil-rock mixture, Environ. Earth. Sci. 75 (2016) 284, https://doi.org/10.1007/s12665-015-5193-x.
[49] H. Zhang, D. Boldini, L. Wang, H. Deng, C. Liu, Influence of block form on the shear behaviour of soft soil–rock mixtures by 3D block modelling approaches, Rock. Mech. Rock. Eng. 55 (2022) 3279–3300, https://doi.org/10.1007/s00603-022-02795-x.
[50] B.E. Wickland, G.W. Wilson, D. Wijewickreme, B. Klein, Design and evaluation of mixtures of mine waste rock and tails, Can. Geotech. J. 43 (9) (2006) 928–945, https://doi.org/10.1139/t06-058.
[51] S. Li, Z. Yang, Y. Gao, H. Liu, X. Liu, X. Jin, Wetting deformation characteristics of soil-rock mixture considering the water-disintegration of red stratum soft rock, Acta Geotech. 19 (2024) 4381–4397, https://doi.org/10.1007/s11440-023-02162-2.
[52] Srinvasa Murthy, B.R., Nagaraj, T.S., Bindumadhava, Influence of coarse particles on compressibility of soils. Proceedings, International Symposium on Prediction and Performance in Geotechnical Engineering, Calagary, Canada, Balkema, Rotterdam. (1987) 601-613.

[53] Y. Wei, Y. Yang, J. Wang, H. Liu, J. Li, Y. Jie, Performance evaluation of high energy dynamic compaction on soil-rock mixture geomaterials based on field test, Case Stud. Constr. Mat. 18 (2023) e01734, https://doi.org/10.1016/j.cscm.2022.e01734.
[54] L. Liu, Y. Yang, X. Mao, M. Nie, Macro-meso shear properties of alluvial-diluvial soil-rock mixture (ADSRM) subgrade fillers based on field investigation and N-method, Case Stud. Constr. Mat. 17 (2022) e01694, https://doi.org/10.1016/j.cscm.2022.e01694.
[55] H. Xu, T.Y. Zhou, X.Y. Wang, J. Zhang, X.B. Zhang, Y.C. Liu, Compression test and numerical simulation research on improved red beds subgrade fillers in Sichuan-Tibet Railway, Rock. Soil Mech. 42 (8) (2021) 2259–2268. ⟨https://rocksoilmech.researchcommons.org/journal/vol42/iss8/9⟩.
[56] B. Indraratna, Q.D. Sun, S. Nimbalkar, Observed and predicted behaviour of rail ballast under monotonic loading capturing particle breakage, Can. Geotech. J. 52 (1) (2015) 73–86, https://doi.org/10.1139/cgj-2013-0361.
[57] W.J. Xu, H.Y. Zhang, Meso and macroscale mechanical behaviors of soil-rock mixtures, Acta Geotech. 17 (2022) 3765–3782, https://doi.org/10.1007/s11440-022-01449-0.
[58] Y.S. Yao, J. Li, J.J. Ni, C.G. Liang, A.S. Zhang, Effects of gravel content and shape on shear behaviour of soil-rock mixture: experiment and DEM modelling, Comput. Geotech. 141 (2022) 104476, https://doi.org/10.1016/j.compgeo.2021.104476.
[59] E. Garzón, P.J. Sánchez-Soto, E. Romero, Physical and geotechnical properties of clay phyllites, Appl. Clay Sci. 48 (3) (2010) 307–318, https://doi.org/10.1016/j.clay.2009.12.022.
[60] ASTM D2216-19, Standard test methods for laboratory determination of water (moisture) content of soil and rock by mass, ASTM International, West Conshohocken, PA, 2019, https://doi.org/10.1520/D2216-19.
[61] ASTM D7263-21, Standard test methods for laboratory determination of density (unit weight) of soil specimens, ASTM International, West Conshohocken, PA, 2021, https://doi.org/10.1520/D7263-21.
[62] ASTM D4318-17e1, Standard test methods for liquid limit, plastic limit, and plasticity index of soils, ASTM International, West Conshohocken, PA, 2017, https://doi.org/10.1520/D4318-17E01.
[63] F. Lanaro, P. Tolppanen, 3D characterization of coarse aggregates, Eng. Geol. 65 (1) (2002) 17–30, https://doi.org/10.1016/S0013-7952(01)00133-8.
[64] ISRM, Suggested method for determining point load strength, Int J. Rock. Mech. Min. Sci. Geomech. (Abstr.) 22 (2) (1985) 51–60, https://doi.org/10.1016/0148-9062(85)92327-7.
[65] T.N. Singh, A. Kainthola, A. Venkatesh, Correlation between point load index and uniaxial compressive strength for different rock types, Rock. Mech. Rock. Eng. 45 (2012) 259–264, https://doi.org/10.1007/s00603-011-0192-z.
[66] M. Heidari, A.A. Momeni, F. Naseri, New weathering classifications for granitic rocks based on geomechanical parameters, Eng. Geol. 166 (8) (2013) 65–73, https://doi.org/10.1016/j.enggeo.2013.08.007.
[67] ASTM C136/C136M-19, Standard test method for sieve analysis of fine and coarse aggregates, ASTM International, West Conshohocken, PA, 2019, https://doi.org/10.1520/C0136_C0136M-19.
[68] ASTM D1557-12, Standard Test Methods for Laboratory Compaction Characteristics of Soil Using Modified Effort (56,000 Ft-Lbf/ft^3 (2,700 kN-m/m^3)), ASTM International, West Conshohocken, PA, 2021, https://doi.org/10.1520/D1557-12R21.
[69] ASTM D2166/D2166M-16, Standard test method for unconfined compressive strength of cohesive soil, ASTM International, West Conshohocken, PA, 2016, https://doi.org/10.1520/D2166_D2166M-16.
[70] Y. Xiao, W. Xiao, H. Wu, H. Zhao, H. Liu, Particle size effect on unconfined compressive strength of biotreated sand, Transp. Geotech. 42 (2023) 101092, https://doi.org/10.1016/j.trgeo.2023.101092.
[71] JTG, Test Methods of Soils for Highway Engineering, 3430-2020, Ministry of Transport of the People's Republic of China, Beijing, 2020.
[72] ASTM D1883-16, Standard Test Method for California Bearing Ratio (CBR) of Laboratory-compacted Soils, ASTM International, West Conshohocken, PA, 2016, https://doi.org/10.1520/D1883-16.
[73] Q. Yang, W. Wen, L. Zeng, H. Fu, Q. Gao, L. Chen, H. Bian, Road performance and prediction model for carbonaceous mudstone soil-rock mixtures under wet-dry cycles, Road. Mater. Pavement 25 (8) (2023) 1–19, https://doi.org/10.1080/14680629.2023.2278146.
[74] Z. Zhang, P. Vadim, N. Svetlana, Z.Q. Zhang, J.J. Wu, Disintegration characteristics of a cryolithogenic clay loam with different water content: Moscow covering loam (prQ_{III}), case study, Eng. Geol. 258 (2019) 105159, https://doi.org/10.1016/j.enggeo.2019.105159.
[75] X. Liu, X. Zhang, L. Kong, G. Wang, J. Lu, Disintegration of granite residual soils with varying degrees of weathering, Eng. Geol. 305 (2022) 106723, https://doi.org/10.1016/j.enggeo.2022.106723.
[76] B.O. Hardin, Crushing of soil particles, J. Geotech. Eng. 111 (10) (1985) 1177–1192, https://doi.org/10.1061/(ASCE)0733-9410(1985)111:10(1177).
[77] Y. Nakata, M. Hyodo, A.F.L. Hyde, Y. Kato, H. Murata, Microscopic particle crushing of sand subjected to high pressure one-dimensional compression, Soils Found. 41 (1) (2001) 69–82, https://doi.org/10.3208/sandf.41.69.
[78] G.R. McDowell, On the yielding and plastic compression of sand, Soils Found. 42 (1) (2002) 139–145, https://doi.org/10.3208/sandf.42.1139.
[79] C. Marone, C.H. Scholz, Particle-size distribution and microstructures within simulated fault gouge, J. Struct. Geol. 11 (7) (1989) 799–814, https://doi.org/10.1016/0191-8141(89)90099-0.
[80] X. Zhang, B.A. Baudet, Particle breakage in gap-graded soil, Geotech. Lett. 3 (2) (2013) 72–77, https://doi.org/10.1680/geolett.13.00022.
[81] S. Wang, X. Gao, W. Ma, K. Zhao, P. Xu, Experimental study on static and dynamic characteristics of geopolymer-stabilized coarse-grained soils, Acta Geotech. 19 (2) (2024) 717–739, https://doi.org/10.1007/s11440-023-01876-7.
[82] X. Si, F. Gong, Strength-weakening effect and shear-tension failure mode transformation mechanism of rockburst for fine-grained granite under triaxial unloading compression, Int. J. Rock. Mech. Min. 131 (2020) 104347, https://doi.org/10.1016/j.ijrmms.2020.104347.
[83] X. Zhang, X. Liu, Y. Xu, G. Wang, Y. Ren, Compressibility, permeability and microstructure of fine-grained soils containing diatom microfossils, Géotechnique 74 (7) (2023) 661–675, https://doi.org/10.1680/jgeot.22.00155.
[84] F.S. Ackah, W. Hailiang, F. Huaiping, L. Cheng, L.Z. Feng, Use of Taguchi method to evaluate the unconfined compressive strength of quicklime stabilized silty clayey subgrade, Case Stud. Constr. Mat. 17 (2022) e01417, https://doi.org/10.1016/j.cscm.2022.e01417.
[85] C. Li, D. Zhang, S. Du, B. Shi, Computed tomography based numerical simulation for triaxial test of soil–rock mixture, Comput. Geotech. 73 (2016) 179–188, https://doi.org/10.1016/j.compgeo.2015.12.005.
[86] X.B. Chen, Z.Y. Li, J.S. Zhang, Effect of granite gravel content on improved granular mixtures as railway subgrade fillings, J. Cent. South Univ. 21 (8) (2014) 3361–3369, https://doi.org/10.1007/s11771-014-2310-z.
[87] L.E. Vallejo, S. Lobo-Guerrero, The shear strength of granular materials containing dispersed oversized particles: DEM analysis, Int. J. Geotech. Eng. 6 (3) (2012) 371–380, https://doi.org/10.3328/IJGE.2012.06.03.371-379.
[88] W.J. Chang, T. Phantachang, Effects of gravel content on shear resistance of gravelly soils, Eng. Geol. 207 (2016) 78–90, https://doi.org/10.1016/j.enggeo.2016.04.015.
[89] H. Li, C. Cui, Y. Sheng, M. Zhang, Z. Feng, L. Li, Y. Zhang, Application of composite steel slag as subgrade Filler: Performance evaluation and enhancement, Constr. Build. Mater. 370 (2023) 130448, https://doi.org/10.1016/j.conbuildmat.2023.130448.
[90] JTG, Technical Specifications for Construction of Highway Subgrades, Ministry of Transport of the People's Republic of China, Beijing, 2019.
[91] W.J. Xu, H.Y. Zhang, Research on the effect of rock content and sample size on the strength behavior of soil-rock mixture, Bull. Eng. Geol. Environ. 80 (2021) 2715–2726, https://doi.org/10.1007/s10064-020-02050-z.
[92] Y. Wang, C.H. Li, Y.Z. Hu, X-ray computed tomography (CT) observations of crack damage evolution in soil-rock mixture during uniaxial deformation, Arab. J. Geosci. 11 (2018) 199, https://doi.org/10.1007/s12517-018-3561-z.
[93] H. Qin, S. Cao, E. Yilmaz, Mechanical, energy evolution, damage and microstructural behavior of cemented tailings-rock fill considering rock content and size effects, Constr. Build. Mater. 411 (2024) 134449, https://doi.org/10.1016/j.conbuildmat.2023.134449.
[94] A. Shakoor, B.D. Cook, The effect of stone content, size and shape on engineering, Environ. Eng. Geosci. xxvii (2) (1990) 245–253, https://doi.org/10.2113/gseegeosci.xxvii.2.245.

[95] T.L. Shelly, D.E. Daniel, Effect of gravel on hydraulic conductivity of compacted soil liners, J. Geotech. Eng. 119 (1) (1993) 54–68, https://doi.org/10.1061/(ASCE)0733-9410(1993)119:1(54).
[96] I.G.B. Indrawan, H. Rahardjo, E.C. Leong, Effects of coarse grained materials on properties of residual soil, Eng. Geol. 82 (3) (2006) 154–164, https://doi.org/10.1016/j.enggeo.2005.10.003.
[97] A. Shafiee, Permeability of compacted granule–clay mixtures, Eng. Geol. 97 (3-4) (2008) 199–208, https://doi.org/10.1016/j.enggeo.2008.01.002.
[98] Y. Wang, S. Zheng, Z. Zhong, Y. Li, Z. Li, Experimental investigation on the hydraulic characteristics of water inrush in deep buried filled karst conduit considering the permeability, Transp. Geotech. 43 (2023) 101115, https://doi.org/10.1016/j.trgeo.2023.101115.
[99] R. Taylor, T. Smith, The engineering geology of clay minerals: swelling, shrinking and mudrock breakdown, Clay Min. 21 (3) (1986) 235–260, https://doi.org/10.1180/claymin.1986.021.3.01.